Modeling Crack Propagation in Rubber

Yoav Lev, Konstantin Volokh

Faculty of Civil and Environmental Engineering, Technion, I.I.T., Israel

Abstract

Traditional bulk failure models are based on the approach of continuum damage mechanics involving internal variables which are difficult to measure and interpret in simple physical terms. Alternative approach was proposed by Volokh [1-5], in which the function of the strain energy density was limited. The limiter enforces saturation – the failure energy – in the strain energy function, which indicates the maximum amount of energy that can be stored and dissipated by an infinitesimal material volume. The limiter induces stress bounds in the constitutive equations automatically.

The work presents a numerical implementation of the energy limiter theory using the LS-DYNA® user defined material. This approach will be tested in few examples. First, the FE subroutine is checked against a simple uniaxial tension case that can be solved analytically. Next, we will model the Deegan-Petersan-Marder-Swinney (DPMS) experiments [6-7] for the dynamic fracture of rubber. These tests use biaxial pre-stretched rubber sheets which are pricked at a point. The pricking initiates a crack which runs along the sheet. We simulate these tests using the user defined subroutines of the hyper-elastic material models enhanced with energy limiters. The numerical results regarding the crack shape and speed are compared to the test observations.

1. Introduction

There are few studies done on the modeling of actual failure and its propagation of rubberlike materials. Theoretical studies for failure mostly focus on the description of deformation using the Linear Elastic Fracture Mechanics (LEFM) theory [8-9]. Theories based on LEFM ignore material and geometrical nonlinearities.

Elastomers or rubberlike materials have unique properties:

- Incompressibility: the bulk modulus is much higher than the shear modulus
- Hyper-elasticity
- Stiffening behavior around high stretches: caused by unfolding of long polymer molecules in the load direction (Figure 1). This behavior is observed in a typical stress-stretch diagram for a uniaxial test on rubberlike materials (Figure 2)

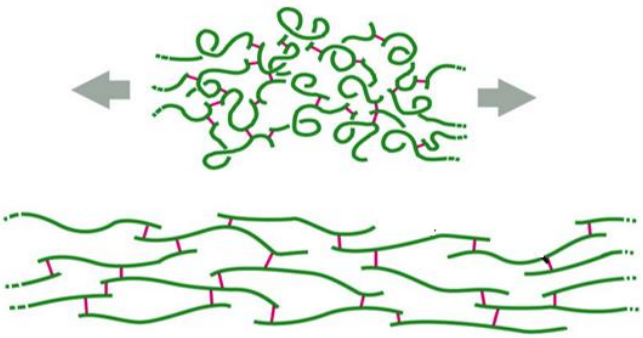

Figure 1: Ilustration of the unfolding of long molecules in the load direction

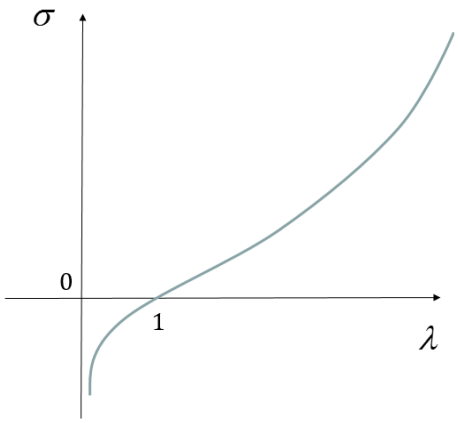

Figure 2: A typical stress-stretch rubberlike behavior for a uniaxial condition

The stress-stretch relation in Figure 2 represents a typical pattern for hyper-elastic models, where the stress has no limit for the increasing stretch. This is unrealistic, of course. Experimental data for uniaxial tension tests on natural rubber vulcanizate show existence of a critical rupture stretch around $\lambda_{cr} \cong 7.0$.

The experimental calibration of damage in traditional theories is far from trivial. It is difficult to measure the damage parameter directly. The experimental calibration should be implicit and it should include both the damage evolution equation and the failure condition. To overcome these difficulties Volokh [1-5] proposed a new approach for modeling rubber fracture based on elasticity with energy limiters. This alternative theory presents the bulk material failure in a more feasible way than the traditional damage theories.

Theory of hyper-elasticity with energy limiters is described in Section 2. Numerical implementation of the theory using the LS-DYNA user defined material is given in Section 3. Section 4 uses the calibrated model for the simulation of DPMS experiments [6-7] for the dynamic fracture of rubber sheets. Section 5 summarizes the work.

2. Elasticity with Energy Limiters

The hyper-elastic constitutive law is defined in the following general form [1-5]

$$\mathbf{P} = \frac{\partial \psi}{\partial \mathbf{F}} \tag{1}$$

where ψ is the Helmholtz free energy (stored energy) per unit reference volume defined as follows

$$\psi(\mathbf{F}, \alpha) = \psi^f - H(\alpha)\psi^e(\mathbf{F}) \tag{2}$$

$$\psi^f = \psi^e(\mathbf{1}) \tag{3}$$

$$\|\mathbf{F}\| \to \infty \;\Rightarrow\; \psi^e(\mathbf{F}) \to 0 \tag{4}$$

where ψ^f and $\psi^e(\mathbf{F})$ designate the constant bulk failure energy and the elastic free energy respectively; $H(\alpha)$ is a unit step function, i.e. $H(z)=0$ if $z<0$ and $H(z)=1$ otherwise; $\mathbf{1}$ is a second-order identity tensor; and $\|...\|$ is a tensor norm.

The switch parameter $\alpha \in (-\infty, 0]$ is defined by the evolution equation

$$\dot{\alpha} = -H\left(\varepsilon - \frac{\psi^e}{\psi^f}\right), \quad \alpha(t=0)=0 \ , \tag{5}$$

where $0<\varepsilon<<1$ is a dimensionless precision constant.

The physical interpretation of (2)-(5) is straightforward: material response is hyper-elastic as long as the stored energy is below its limit, ψ^f. When the limit is reached, the stored energy remains constant for the rest of the deformation process, thereby making material healing impossible. Parameter α is not an internal variable (like in Damage Mechanics); it functions as a switch: if $\alpha=0$ then the process is elastic and if $\alpha<0$ then the material is irreversibly damaged and the stored energy is dissipated.

In order to enforce the energy limiter in the stored energy function, we use the following form of the elastic energy

$$\psi^e(\mathbf{F}) = \frac{\phi}{m}\Gamma\left(\frac{1}{m}, \frac{W(\mathbf{F})^m}{\phi^m}\right) \tag{6}$$

where $\Gamma(s,x)=\int_x^\infty t^{s-1}s^{-t}dt$ is the upper incomplete gamma function; $W(\mathbf{F})$ is the stored energy of intact (without failure) material; ϕ is the energy limiter, which is calibrated in macroscopic experiments; and m is a dimensionless material parameter, which controls the sharpness of the transition to material failure on the stress-strain curve. Increasing or decreasing m it is possible to simulate more or less steep ruptures of the internal bonds accordingly.

The failure energy can be calculated via (3) as follows

$$\psi^f = \psi^e(\mathbf{1}) = \frac{\phi}{m}\Gamma\left(\frac{1}{m}, \frac{W(\mathbf{1})^m}{\phi^m}\right) \tag{7}$$

Substitution of (2), (6), (7) in (1) yields

$$\mathbf{P} = -H(\alpha)\frac{\partial \psi^e}{\partial \mathbf{F}} = \exp\left(-\frac{W^m}{\phi^m}\right)H(\alpha)\frac{\partial W}{\partial \mathbf{F}} \tag{8}$$

Choosing as an example the Yeoh strain-energy function and using the experimental data found from Hamdi et al [8] for Natural Rubber (NR) vulcanizate we have

$$W = \sum_{k=1}^{3} c_k \left(I_1 - 3\right)^k \tag{9}$$

where the material parameters

$$c_1 = 0.298\,MPa \quad c_2 = 0.014\,MPa \quad c_3 = 0.00016\,MPa \tag{10}$$

the energy limiter ϕ = 79.9 MPa and the material parameter $m = 10$ are deduced from the material failure at the critical stretch of $\lambda_{cr} = 7.12$ observed from the test.

The Cauchy stress is determined by

$$\boldsymbol{\sigma} = \left(\det \mathbf{F}\right)^{-1} \mathbf{P}\mathbf{F}^{T} \tag{11}$$

The Cauchy stress - stretch curve for the NR model described by equations (8-11) is shown in Figure 3, where also the results are shown for the intact model where no failure exists ($\phi \to \infty$).

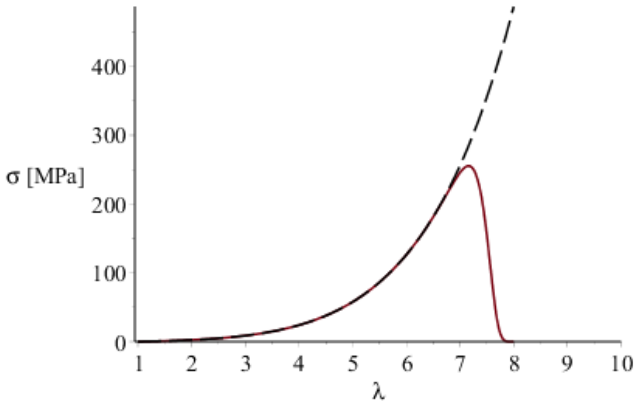

Figure 3: Cauchy stress [MPa] versus stretch in uniaxial tension of NR: dashed line designates the intact model; solid line designates the model with the energy limiter

Hamdi et al. [10] have also conducted biaxial tests up to rapture with the same rubber material used for the uniaxial test. A comparison between the tests and the predicted theory results of the critical failure stretches, λ_{1cr} and λ_{2cr}, for the biaxial case are presented in Figure 4.

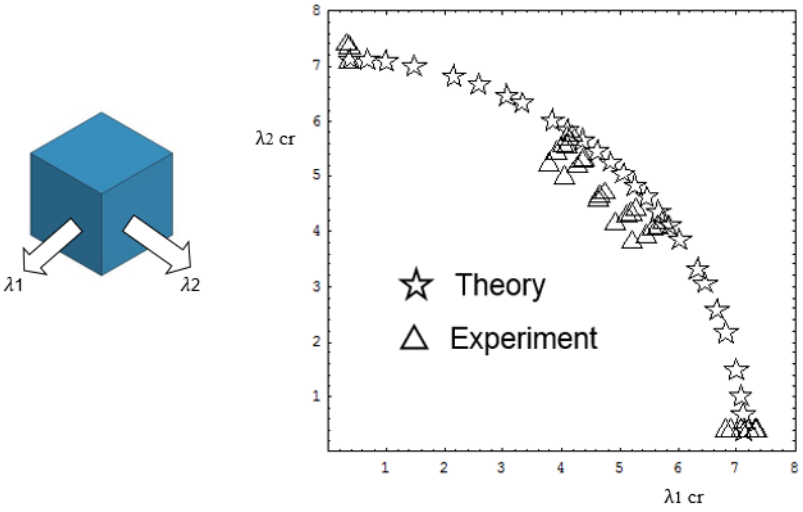

Figure 4: Critical failure stretches in biaxial tension

The comparison of the numerical to the test results for the biaxial case shows a close resemblance, although the energy limiter used was found from the calibration to the uniaxial test.

3. LS-DYNA User Defined Material Implementation

The simulations in our work are done by using the explicit dynamics version of the LS-DYNA finite element software [11]. User-defined subroutine of the hyper-elastic material model enhanced with the energy limiter are plugged in. The simulation process also includes the deletion of the failed elements based on a criterion and the LS-DYNA built-in commands. The deletion of elements from the mesh enforces dissipation computationally. This is important in dynamics where the elastic unloading can potentially lead to the healing of the failed material. By removing the failed elements from the mesh we prevent the healing and account for dissipation.

The deletion of the elements occurs when the following failure criterion is obeyed:

$$H(\alpha) = 0 \tag{12}$$

Since we are dealing with the explicit method we cannot use the fully incompressible theory as presented and we slightly modify the strain energy function described in (2) in order to penalize volumetric changes:

$$\hat{\psi} = \psi + \alpha(I_3 - 1) - \beta \ln I_3 \tag{13}$$

where $I_3 = \det \mathbf{C}$, and α and β are material constants. Using the condition of zero residual stresses where $\boldsymbol{\sigma}(\mathbf{F} = \mathbf{1}) = \mathbf{0}$ we can find the relation between the material constants. The FE subroutine is checked against analytical results of the uniaxial tension case.
Using for example the Biderman strain energy model

$$W = \left(\sum_{k=1}^{3} c_k (I_1 - 3)^k \right) + c_{01}(I_2 - 3) \tag{14}$$

with material constants taken from Marckmann G, Verron E [12]

$$c_1 = 0.208\,MPa,\ c_2 = -0.0024\,MPa,\ c_3 = 0.0005\,MPa,\ c_{01} = 0.0233\,MPa \tag{15}$$

The energy limiter ϕ = 69.2 MPa is found assuming the critical stretch $\lambda_{cr} = 7$, and the material parameter $m = 10$ (a real uniaxial tension test is needed for exact values of these parameters).

We have an excellent correlation between the analytical and numerical results for the Cauchy stress vs. stretch (Figure 5).

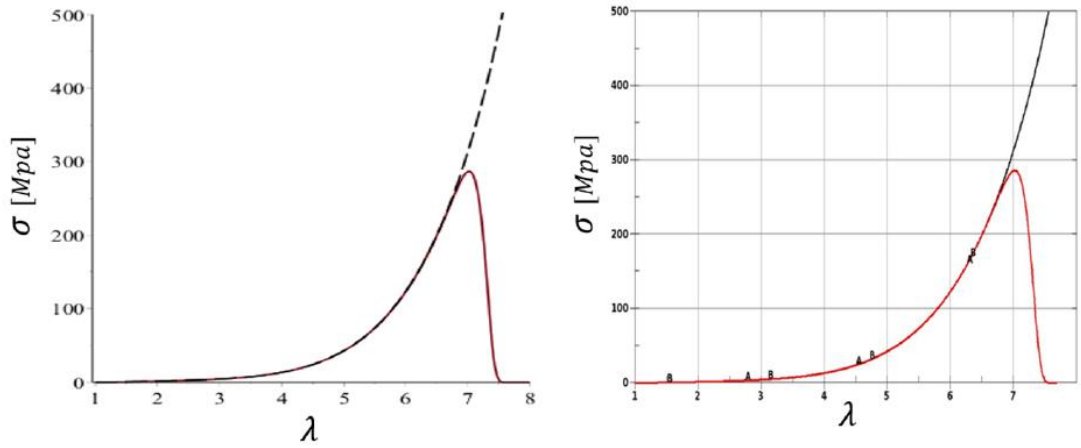

Figure 5: Cauchy stress vs. stretch in uniaxial tension. Left - analytical results, Right - LS-DYNA results

The discretization of the upper incomplete Gamma function - Γ included in the strain energy function in (6) and (7) is done by inserting written subroutines by Shanjie Zhang and Jianming Jin [13]. A comparison between numerical and analytical maximum value of the strain energy - ψ from (2) for different values of m are presented in
Table 1.

	Analytical	Numerical (LS-Dyna)
m	[MPa]	
5	63.56	63.56
10	65.86	65.86
20	67.40	67.40
100	68.84	68.84

Table 1: Maximum ψ comparison for different values of m for uniaxial case

The comparison shows an excellent fit with no difference in values (at least up to the second number after the decimal point).

The evolution of the elastic energy - ψ^e from (6), the failure energy ψ^f from (7), the proposed strain energy function - ψ from (2), and the classical strain energy function W from (14) are presented in Figure 6.

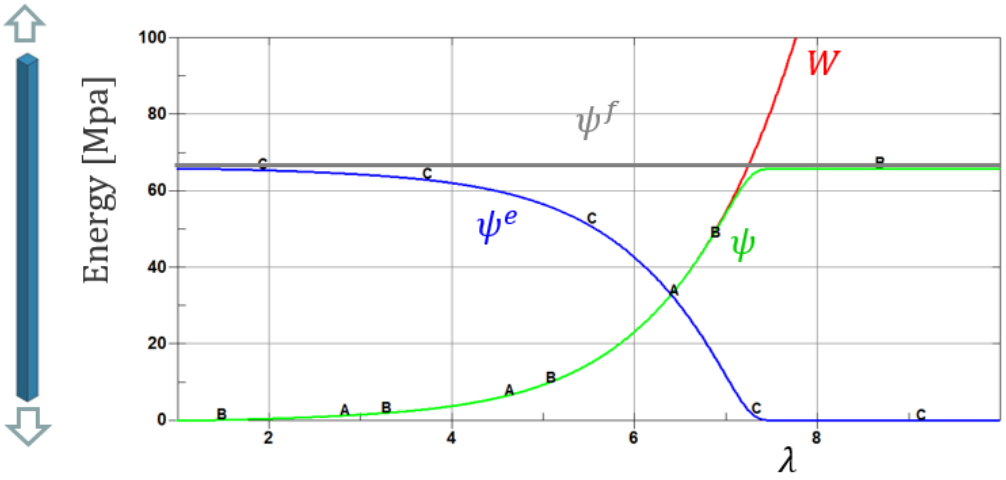

Figure 6: Different energy variables vs. stretch for the uniaxial tension case

4. Simulating the Deegan-Petersan-Marder-Swinney (DPMS) Experiments

We will now use the calibrated user defined subroutine for modeling multi degrees of freedom analysis. Propagation of cracks in natural rubber was investigated in DPMS experiments [6-7].

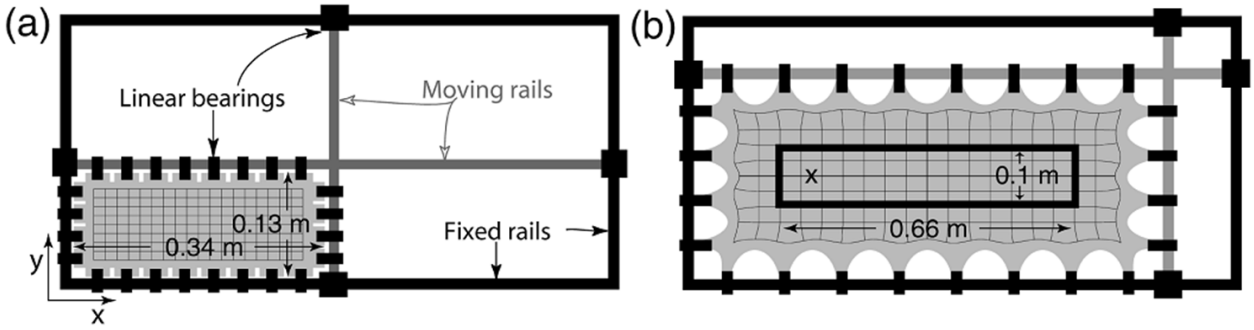

Figure 7: The experimental apparatus for biaxial stretching of rubber sheet [7]

The experimental apparatus included the framework for the biaxial pre-stress of the rubber sheet. After stretching, the sheet is clamped by the inner frame and pricked at the point marked with 'x' (Figure 7). The pricking initiates a crack which runs along the sheet. DPMS tests made many interesting observations of the running crack. Using a high speed camera, they measured the shape and velocity of the crack as function of the initial biaxial stretch value. The reported speed of the running crack varies between 37 and 60 m/sec.

For the numerical model of the DPMS experiments we use a rectangle with a thickness of 0.05 mm which is the same thickness mentioned in the tests. The length and width of the rectangle in the model are 39.6 mm and 11.5 mm accordingly (smaller than the actual dimensions in order to save CPU time). We use one element to the thickness making a total of 112,640 Hexa (8 node) element (Figure 8). The rectangle is fixed around the boundaries.

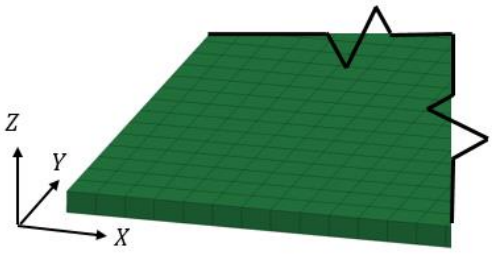

Figure 8: Mesh of the rectangular model

We start with the Biderman model where the energy limiter is presented in section 3 (14-15).
The chosen initial stretch values are $\lambda_x = 2.0$ $\lambda_x = 4.0$ $\lambda_z = 1/(\lambda_x \lambda_y) = 0.125$.
At the beginning of the analysis a line of a few elements is deleted (Figure 9)

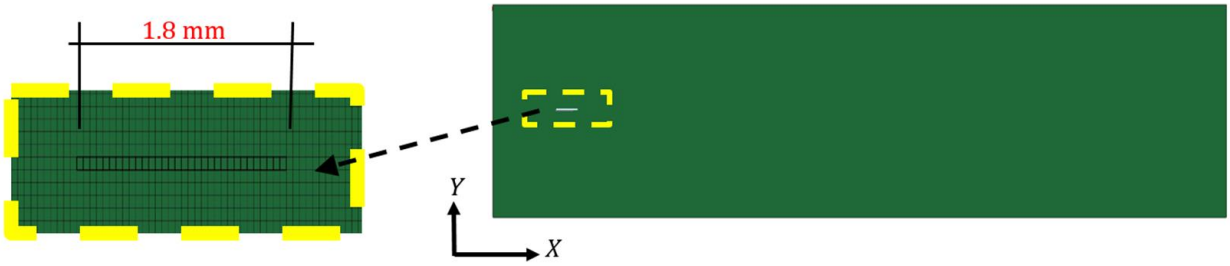

Figure 9: Initial elements deleted

After deletion of the initial elements, the crack propagates spontaneously (Figure 10)

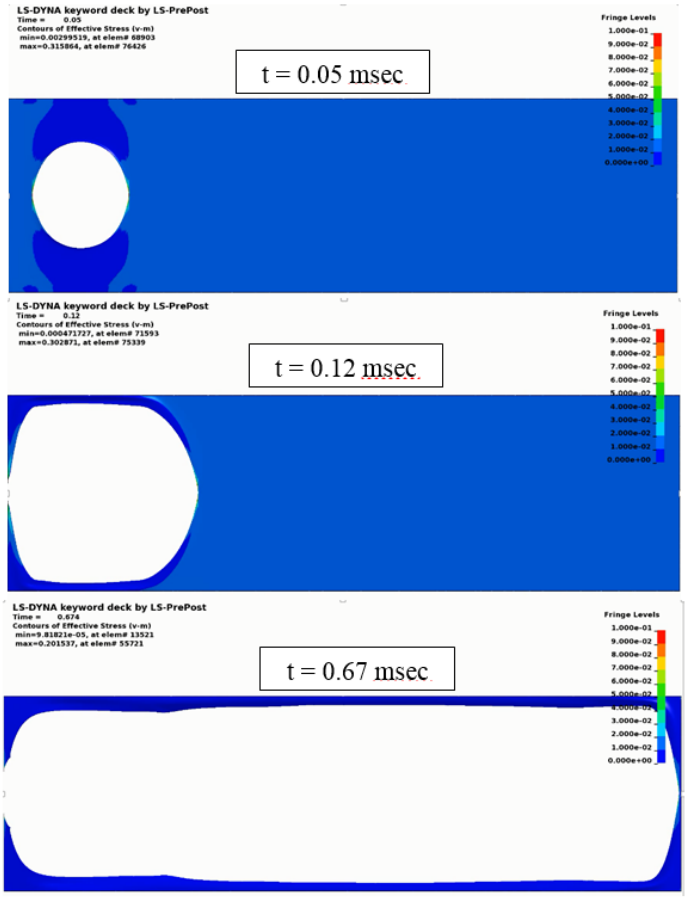

Figure 10: Numerical results of the crack at different durations from start

The speed of the crack tip calculated from the results is 51 m/sec, showing a good correlation with the rate of crack tip speed reported in Petersan's tests (37 to 60 m/sec).
A good correlation is also achieved for the crack tip shape (Figure 11).

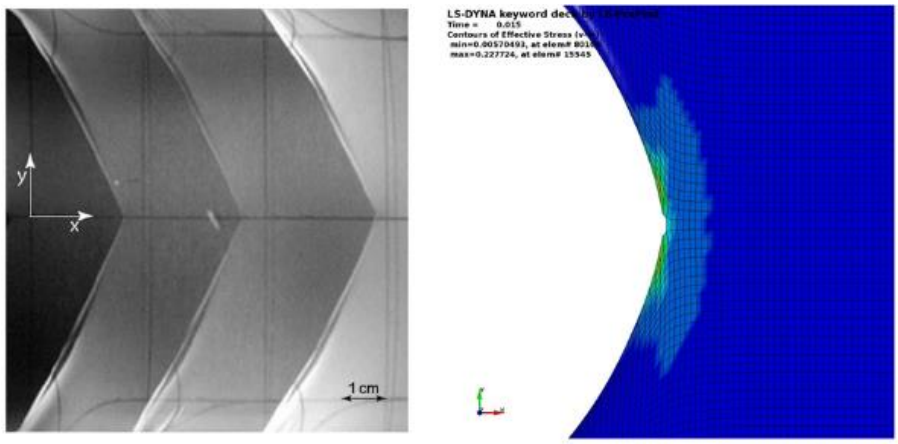

Figure 11: Snapshot of crack tip. Left - Petersan's tests. Right - numerical analysis

Displaying only the deleted elements (without any deformation) shows a straight line (Figure 12).

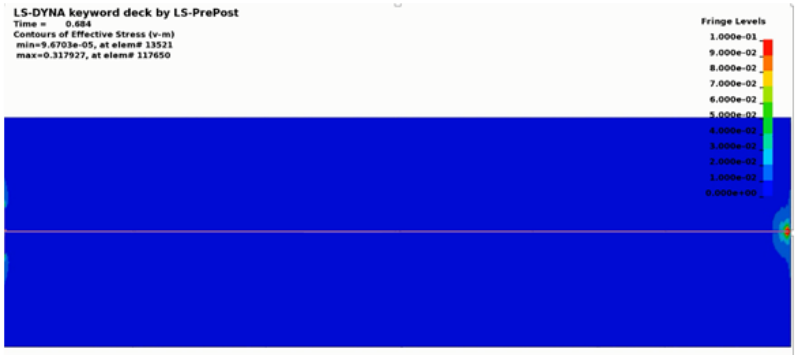

Figure 12: Deleted elements view – Biderman model

Repeating the simulations for the material mentioned in section 2 in (9) and (10) for the Yeoh model (material constants in this case are stiffer), the speed of the crack is 81.7 m/sec and the crack shape shows a splitting nature (Figure 13) opposed to the straight line in the previous example (Figure 12).

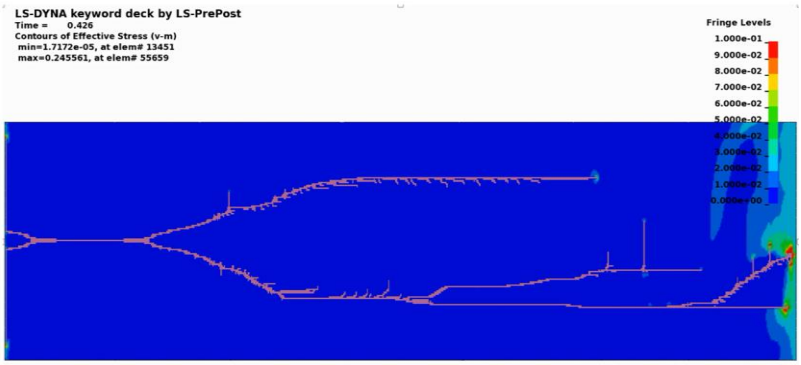

Figure 13: Deleted elements view - Yeoh model

Checking the mesh dependency on the behavior of the running crack we prepared 3 different mesh sizes for the model (Figure 14). The same area of elements are initially deleted in all 3 cases for the initiation of the crack

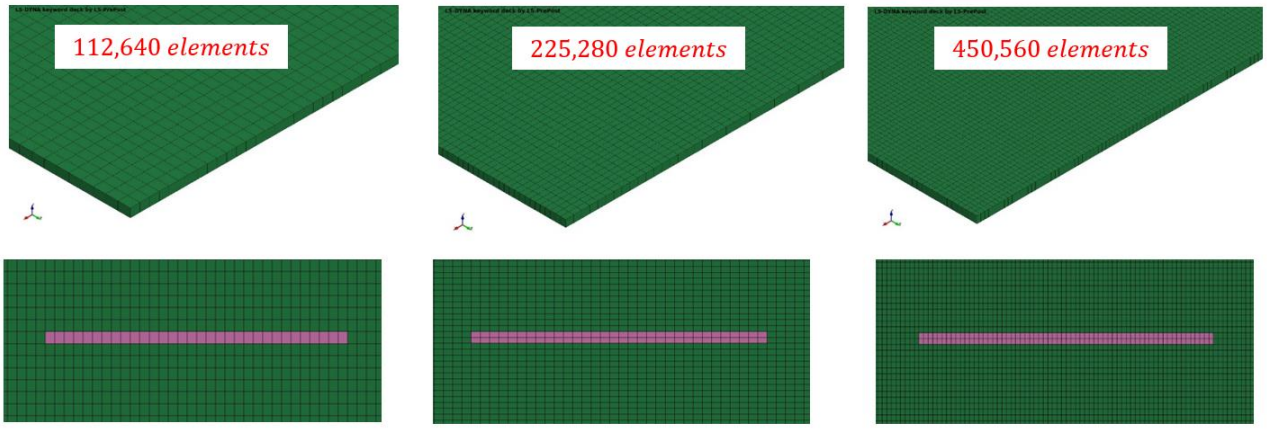

Figure 14: Three different mesh size and initial deleted elements

Figure 15 is a snap shot of the crack 0.18 msec after initiation for the 3 mesh size options.

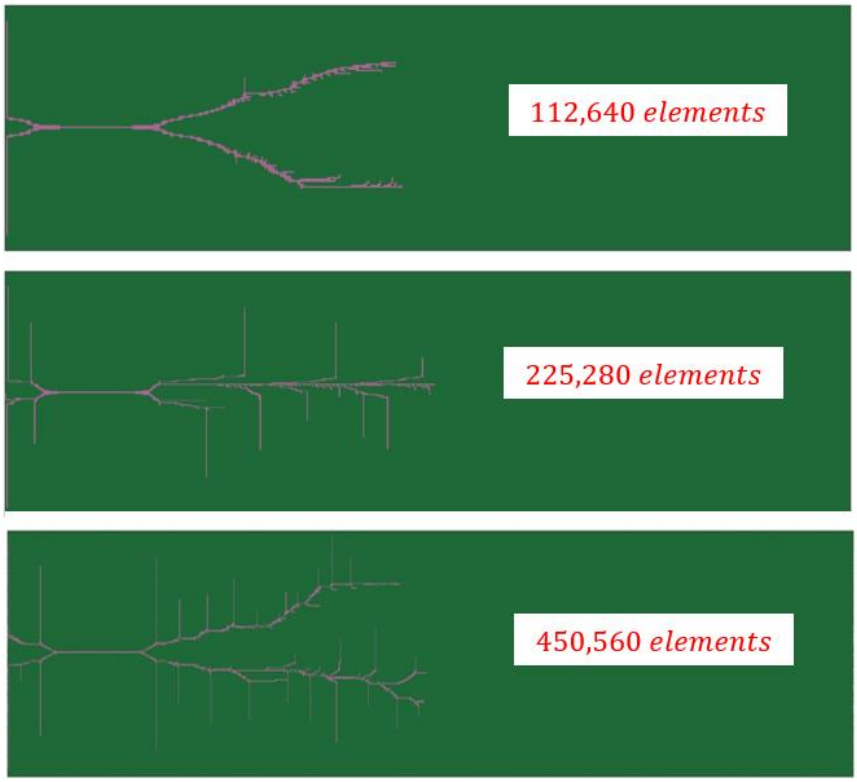

Figure 15: Crack shape after 0.18 msec for 3 different mesh size

The resulting running crack has almost the same speed for the 3 mesh types. However, the deleted elements show different evolution paths.

The dependency of the mesh size on the deleted elements is a well-known problem in using the FE method. It occurs at the point where the stiffness becomes negative, which results in local straining that is dependent on mesh size. Future study is planned for the implementation of a suitable regularization method.

5. Summary

The general objective of this work is to advance the modeling of rubber fracture and to get new insights into the core problems of fracture mechanics based on the approach of elasticity with energy limiters [1-5]. This approach includes a description of a maximum energy that can be accumulated in an infinitesimal material volume. The method is dramatically simpler than existing methods that include sophisticated approaches of damage mechanics involving internal variables.

The simulations presented are done using the explicit dynamics version of the LS-DYNA finite element software. User-defined subroutines of the hyper-elastic material models enhanced with the energy limiters are plugged in. Although the energy limiter is found from the calibration to a uniaxial tension test, the prediction to a biaxial tension test has proved to be successful.

Using the user defined subroutine for simulating the running crack for the biaxial stretched rubber sheet conducted by DPMS tests [6-7] we have demonstrated the following:

- Resemblance to the crack tip shape
- Resemblance to the crack velocity
- Crack speed is a function of the material model
- Finer mesh has very small influence on the crack speed
- Finer mesh changes the crack structure (regularization method is needed)

It is hoped that the numerical simulations of the experiments will advance our understanding of the key issues on fracture, and enable improving the design of structural elements made out of rubber.

References

[1] Volokh KY (2007) Hyper-elasticity with softening for modeling materials failure. J Mech Phys Solids 55:2237-2264
[2] Volokh KY (2010). On modeling failure of rubberlike materials. Mech Res Commun 37:684-689
[3] Volokh KY (2011) Cavitation instability in rubber. Int J Appl Mech 3:299-311
[4] Volokh KY (2013) Review of the energy limiters approach to modeling failure of rubber. Rubber Chem Technol 86:470-487
[5] Volokh KY (2014) On irreversibility and dissipation in hyperelasticity with softening. J Appl Mech 81:074501
[6] Deegan, R.D., Petersan, P.J., Marder, M., Swinney, H.L., (2001). Oscillating fracture paths in rubber. Phys. Rev. Lett. 88, 014304
[7] Petersan, P.J., Deegan, R.D., Marder, M., Swinney, H.L., (2004). Cracks in rubber under tension exceeds the shear wave speed. Phys. Rev. Lett. 93, 015504
[8] Geubelle, P.H., and Knauss, W.G., (1994 a,b,c). Finite strain at the tip of the crack in a sheet of hyper-elastic material. J. Elasticity 35, 61-174
[9] Knowles, J.K., and Sternberg, E., (1983). Large deformations near the tip of an interface crack between two neo-Hookean sheets. J. Elasticity 13, 257-293
[10] Hamdi, A., Nait, A.M., Hocine, N.A., Heuillet, P., Benseddiq, N., 2006. A fracture criterion of rubber-like materials under plane stress conditions. J. Polymer Testing 25, 994-1005
[11] LS-DYNA Keyword User's Manual, Version 971, Livermore Software Technology Corporation, 2012
[12] Marckmann G, Verron E (2006) Comparison of hyper-elastic models for rubber-like materials. Rubber Chem Technol 79:835-858
[13] Shanjie Z., Jianming J., (1996). Computation of Special Functions. Wiley